

1 Technical note: Inference in hydrology from entropy balance considerations

2

3 Stefan J. Kollet

4

5 IBG-3, Institute for Bio- and Geosciences, Research Centre Jülich, Jülich, Germany

6 Centre for High-Performance Scientific Computing in Terrestrial Systems, Geoverbund ABC/J, Germany

7

8 Correspondence to: S. Kollet (s.kollet@fz-juelich.de)

9

10 **Abstract**

11 In this study, the method of inference of macroscale thermodynamic potentials, forces and exchange
12 coefficients for variably saturated groundwater flow is outlined based on the entropy balance. The
13 theoretical basis of the method of inference is the explicit calculation of the internal entropy production
14 from microscale, thermodynamic flux-force relationships using e.g. hyper-resolution variably saturated
15 groundwater flow models. Emphasis is placed on the two-scale nature of the entropy balance equation
16 that allows incorporating simultaneously movement equations at the micro- and macroscale. The
17 method is illustrated with simple hydrologic cross-sections at steady state and periodic sources/sinks at
18 dynamic equilibrium, and provides a thermodynamic point of view of upscaling in variably saturated
19 groundwater flow. The current limitations in the connection with observable variables and predictive
20 capabilities are discussed, and some perspectives for future research are provided.

21

22

23 **Introduction**

24 The current earth sciences literature indicates that entropy balance considerations have been mainly
25 applied in the context of optimality and self-organization. Theories of optimality and self-organization
26 are appealing when dealing with complex non-linear systems, because of their apparent usefulness in
27 interpreting interactions of gradients and fluxes and in quantifying (predicting) systems' states and
28 uncertainties. In this context, the entropy and energy balance received attention, because of its physics-
29 based foundation in non-equilibrium thermodynamics and potential connection with information theory
30 (e.g., Dewar 2003, Koutsoyiannis 2014). The entropy balance appears to be useful in applications to
31 hydrologic (e.g., Zehe et al. 2013, Ehret et al. 2014), ecohydrologic (e.g., Dewar 2010, Miedziejko and
32 Kedziora 2014, del Jesus et al. 2012), and atmospheric sciences (e.g., Paillard and Herbert 2013), and in
33 general to open complex nonlinear thermodynamic systems (Abe and Okuyama 2011).

34 The entropy balance states that in an open system, the change in entropy equals the internal production
35 of entropy minus the divergence of the entropy current. A dynamic equilibrium or steady state is
36 obtained, when entropy production inside (due to e.g. flow processes of heat or matter) equals the
37 divergence of the entropy current i.e. the entropy exchange with the outside. Note also, dynamic
38 equilibrium refers to a state of stationarity in the statistical sense. Optimality of the dynamic equilibrium
39 may be achieved, because the gradient, which drives the flux and, thus the production of entropy, is
40 reciprocally depleted by the same flux (Kleidon et al. 2013).

41 In hydrology, the entropy balance has been applied to conceptual problems based on the overarching
42 rationale that entropy production is maximized (maximum entropy production, MEP) in obtaining a state
43 of dynamic equilibrium by optimizing the fluxes and gradients in competition via an adjustment of some
44 (non-)linear exchange coefficient. There have been some studies demonstrating how entropy production
45 can be maximized by optimizing an exchange coefficient to obtain an optimal system's state. In
46 hydrology, there are quite a few examples of the application and discussion of the MEP principle (e.g.,

47 Ehret et al. 2014, Westhoff et al. 2014, Kleidon and Schymanski 2008) also in connection with data (e.g.,
48 Zehe et al. 2013). However, its validity and applicability to hydrologic systems is still in question
49 (Westhoff and Zehe 2013).

50
51 Often the entropy balance has been applied at steady state with simple bucket models, which are well-
52 mixed (i.e. without internal gradients). For example, Porada et al. (2011) performed a detailed entropy
53 production analysis of the land surface hydrologic cycle including the shallow vadose zone assuming
54 vertical equilibrium of the soil bucket model. Applying linear bucket models without considering internal
55 gradients, Kleidon and Schymanski (2008) showed that if the natural system possesses enough degrees
56 of freedom, in case of steady state, the system will tend towards a certain exchange coefficient, when
57 entropy production is maximized. For similar bucket models, Westhoff et al. (2014) demonstrated the
58 impact of periodic boundary forcing on entropy production, which may result in more than one
59 maximum for unique values of the exchange coefficient at dynamic equilibrium. Interestingly, these
60 studies did not calculate the internal entropy production explicitly. Instead, entropy production was
61 estimated indirectly from the exchange with the outside (i.e. the divergence of the entropy current).

62 In order to optimize effective values of a simple two-box model, Schymanski et al. (2010) recognized the
63 potential of explicitly estimating the internal entropy production using a simple distributed model of the
64 water and carbon balance (Klausmeier 1999), which is based on coupled equations of moisture and
65 biomass and is able to produce vegetation patterns. This study highlights an interesting aspect of
66 entropy balance considerations that is the inference of upscaled effective parameters and state variables
67 to represent subgrid scale variability in coarse scale (macroscale) models. Thus, ultimately, the appeal of
68 the entropy balance maybe the inference of upscaled or effective exchange coefficients and
69 forces/gradients, which may be used to quantitatively describe the complex system without the explicit
70 knowledge about microscopic details (Dewar 2009). In this context, a popular example is gas diffusion,

71 which can be captured by an inferred, macroscopic diffusion coefficient and gradient instead of honoring
72 the motion and interactions of individual molecules.

73 In this study, the method of inference of effective hydrologic exchange coefficients, potentials and forces
74 is outlined using the entropy balance equation in applications to simple hydrologic cross-sections. The
75 purpose of this study is to direct attention to the potential insights gained from a new branch of
76 theoretical hydrology combining modern thermodynamic principles with numerical experiments. While
77 the thermodynamic principles constitute the link between different spatial scales that may be useful in
78 upscaling hydrologic process across a hierarchy of scales, the numerical experiments constitute the
79 methodological pillar to obtain explicitly the internal entropy production or dissipation required in the
80 upscaling, equivalent to *ab initio* simulations in molecular dynamics (Kresse and Hafner 1994). The
81 following sections provide the basic theory with an emphasis on the two-scale nature of the entropy
82 balance, and the application to the hydrologic cross-sections with ensuing discussion and conclusions.

83

84 **Basic theory and the two-scale nature of the entropy balance**

85 The theory outlined in Kondepudi and Prigogine (2015) is applied to the problem of variably saturated
86 groundwater flow at constant temperature. Based on conservation of energy (and the balance equation
87 for concentrations, which is not required in this analysis) Kondepudi and Prigogine (2015) write the
88 entropy balance as follows

$$89 \quad s' + \nabla \cdot J_s = \sigma \quad (1),$$

90 where s' ($\text{ML}^{-1}\text{T}^{-3}\text{K}^{-1}$) is the change in the entropy density with time; J_s ($\text{MT}^{-3}\text{K}^{-1}$) is the entropy current per
91 unit volume; and σ ($\text{ML}^{-1}\text{T}^{-3}\text{K}^{-1}$) is the internal entropy production per unit volume, which is always
92 positive by definition. Thus, the change of entropy density with time of a macroscopic volume depends
93 on the divergence of the entropy current and the internal entropy production.

94 In the considered case of variably saturated groundwater flow, $J_s = JM/T$, where $J(\text{ML}^{-2}\text{T}^{-1})$ is the mass
 95 flow per unit area, $M(\text{L}^2\text{T}^{-2})$ is the chemical potential (i.e. the sum of pressure and gravitational potential,
 96 equation 5) at the macroscale and T (K) is the temperature. At the microscale, defining q ($\text{ML}^{-3}\text{T}^{-1}$) and f
 97 (L^2T^{-2}) as the fluxes and thermodynamics forces per unit volume, the divergence of the entropy current
 98 and the internal entropy production can be expanded as follows

$$99 \quad s' + (M/T)(\nabla \cdot J) + J \cdot (\nabla(M/T)) = \sum qf/T \quad (2).$$

100 For the derivations below it is important to recognize that equation (2) exhibits the unique
 101 characteristics of incorporating two scales: the entropy density change with time and divergence of the
 102 entropy current at the macroscale (all terms on the left hand side), and the entropy production at the
 103 microscale i.e. the sum of all products of the internal microscopic fluxes and forces (term on the right
 104 hand side). Note, in the following, the temperature T (K) is omitted in the equations and units, because
 105 $T = \text{constant}$ in the following derivations.

106 Performing an entropy balance at steady state leads to

$$107 \quad M(\nabla \cdot J) + J \cdot (\nabla M) = \sigma \quad (3)$$

108 because $s' = 0$. In contrast, performing an entropy balance under the influence of periodic external
 109 forcing requires integration over one full forcing cycle at dynamic equilibrium of equation 2 indicated by
 110 overbars

$$111 \quad \overline{M(\nabla \cdot J)} + \overline{J \cdot (\nabla M)} = \bar{\sigma} \quad (4).$$

112 with $\overline{s'} = 0$ over one full cycle. Both approaches will be applied in the following sections, in order to
 113 arrive at effective variables at the macroscale.

114 Because of the two-scale nature of equations 1 and 2, movement equations are introduced at the
115 macroscale and microscale. At the macroscale, $M(L^2T^{-2})$ is defined as the sum of the macroscopic
116 pressure potential $\Psi (L^2T^{-2})$, and gravitational potential $gz(L^2T^{-2})$, leading to

$$117 \quad M = \Psi + gz \quad (5);$$

118 and is, thus, equivalent to the hydraulic head; (∇M) symbolizes a macroscopic thermodynamic force F
119 (L^2T^{-2}) being the difference in the macroscopic chemical potentials

$$120 \quad (\nabla M) = F = M_{high} - M_{low} \quad (6);$$

121 and, at the moment, J is defined as a conductance concept

$$122 \quad J = \lambda F \quad (7),$$

123 where $\lambda (ML^{-4}T)$ is a conductance coefficient ($\lambda = \rho r_s$, with water density $\rho (ML^{-3})$ and resistance $r_s (TL^{-1})$)
124 relating the flux with the force at the macroscale.

125 At the microscale, the chemical potential $\mu, (L^2T^{-2})$, the mass flux $q (ML^{-3}T^{-1})$ per unit volume and the
126 thermodynamic force $f(L^2T^{-2})$ are

$$127 \quad \mu = \psi + gz \quad (8),$$

128 where $\psi (L^2T^{-2})$ is the microscale pressure potential;

$$129 \quad q = \frac{1}{\alpha} \rho \frac{K}{\nu} k_r(\psi)(\mu_{high} - \mu_{low}) \quad (9),$$

130 where $\rho (ML^{-3})$ is the density; $\nu (L^2T^{-1})$ is the kinematic viscosity; K is the permeability (L^2) , $k_r(\psi) (-)$ is the
131 relative permeability, and $\alpha (L^{-2})$ is the unit microscopic flow-through area; and the microscale force

$$132 \quad f = (\mu_{high} - \mu_{low}) \quad (10).$$

133 Technically, $\sum qf$ is the sum of all fluxes and forces (always positive, because any flux produces entropy)
134 between all neighboring cells or elements in a microscale, numerical, variably saturated groundwater
135 flow model including Dirichlet and/or Neumann boundary conditions.

136 Thus, the two-scale nature of equation 2 allows to apply different thermodynamic flux-force
137 relationships at the different scales that are the conductance concept at the macroscale (equation 7) and
138 essentially Darcy's law or Richards equation (equation 9) at the microscale. In equation 2, the entropy
139 production serves as an "automatic" spatial and also temporal integrator of the microscale fluctuations.
140 These two characteristics are remarkable. Note, the calculation (integration) of the entropy balance may
141 be performed over the global domain of volume V (L^3) or any subdomain V_i (L^3) thereof.

142

143 **Method of Inference**

144 The basis of the method of inference is that the internal, microscopic entropy production σ and also the
145 complete entropy balance can be calculated from support scale simulations by implementing the
146 microscale equations 9 and 10 in combination with a continuity equation over the macroscopic domain.
147 In obtaining σ explicitly, one is able to estimate effective potentials, forces and conductance coefficients
148 of equation 7 at the macroscale from the explicitly resolved fluctuations at the microscale, which are
149 thermodynamically consistent. In order to illustrate the method of inference of macroscale potentials,
150 conductances and forces, a number of illustrative examples based on simple hydrologic profiles are
151 presented applying different boundary conditions and source/sink terms.

152

153 *Example 1:*

154 Directed at a heat flow example in Kondepudi and Prigogine (2015), a simple cross-section is considered
 155 (figure 1) with steady-state, variably saturated groundwater flow, J , from left to right due to Dirichlet
 156 boundary conditions on the left M_l and right M_r , with $M_l > M_r$. Because $\nabla \cdot J = 0$, and $s' = 0$ at steady
 157 state, integration of the entropy balance over the cross-section leads to

$$158 \quad S'_i = \int_0^{L_z} \int_0^{L_x} \sigma(x, z) dx dz = L_z \int_0^{L_x} J_x (\nabla_x M) dx \quad (11a)$$

$$159 \quad S'_i = L_z J_x (M_l - M_r) = L_z J_x F \quad (11b),$$

160 where L_z and L_x (L) are the constant vertical and horizontal extents of the cross-section, respectively; S'_i
 161 is the total internal entropy production; and $F = (M_l - M_r)$ is the macroscopic force. Note, in the
 162 following, the entropy production integral is simply written as $S'_i = \int \sigma$, and L_z is lumped into the flux
 163 $L_z J_x = J$ for convenience.

164 In case of this simple example, applying $J = \lambda(M_l - M_r)$ from equation 5, one obtains the expression for
 165 the effective conductance

$$166 \quad \lambda = S'_i (M_l - M_r)^{-2} = S'_i F^{-2} \quad (12)$$

167 and the effective force

$$168 \quad F = S'_i J^{-1} \quad (13).$$

169 Thus, one may obtain the effective conductance for any kind of heterogeneity (i.e. microscale
 170 fluctuations) by explicitly calculating σ and S'_i based on equations 6 and 7 and the macroscopic
 171 boundary conditions M_l and M_r . Note, entropy production is simply the sum of the product of the steady
 172 state fluxes and incremental forces over the cross-section

$$173 \quad S'_i = \int \sigma = \int (\sum qf) = \int \left(\sum \frac{1}{\alpha} \rho \frac{K}{v} k_r(\psi) (\mu_{high} - \mu_{low})^2 \right),$$

174 where individual values of qf are calculated with equations 9 and 10 between two adjacent microscale elements in support scale numerical

175 simulations. While λ could have been obtained directly from the macroscopic flux and the applied
176 boundary conditions similar to a numerical Darcy experiment, the example serves to illustrate the basic
177 concept of inference arriving at a thermodynamic expression for λ and the force F (if a flux is prescribed
178 at the boundaries).

179

180 *Example 2:*

181 This example expands example 1 to steady state groundwater flow including recharge represented by
182 the mass rate Q_s

$$183 \quad Q_s = \int_0^L (\nabla \cdot J) dx \quad (14),$$

184 and integration leading to

$$185 \quad MQ_s + J_l M_l - J_r M_r = S'_i \quad (15).$$

186 where M is the macroscopic potential of the cross-section.

187 The general expression for the macroscopic potential of the cross-section is

$$188 \quad M = Q_s^{-1} (S'_i - (J_l M_l - J_r M_r)) \quad (16).$$

189 In this example, three special cases are considered, namely $J_l = 0$, $J_l < 0$, and $J_l > 0$. In case of $J_l = 0$
190 (figure 2), there is a no-flow boundary condition on the left side resulting in $J_r = Q_s$ and, thus

$$191 \quad M = S'_{i,J_l=0} Q_s^{-1} + M_r \quad (17)$$

$$192 \quad F = (M - M_r) = S'_{i,J_l=0} Q_s^{-1} \quad (18)$$

193 where the subscript indicates the respective case for the left boundary flux.

194 With equation 7 and $J_r = Q_s = J$ follows for the conductance coefficient

$$195 \quad \lambda = S'_{i,J_l=0} F^{-2} \quad (19).$$

196 For $J_l < 0$ (figure 3), the symmetric case is considered, where the potentials at the boundaries are equal

197 ($M_l = M_r = M_b$) and Q_s is uniform over the profile ($-J_l = J_r = Q_s/2$) leading to

$$198 \quad M Q_s - 1/2 Q_s M_l - 1/2 Q_s M_r = S'_{i,J_l < 0} \quad (20a).$$

$$199 \quad Q_s (M - (M_l + M_r)/2) = S'_{i,J_l < 0} \quad (20b).$$

$$200 \quad Q_s (M - M_b) = S'_{i,J_l < 0} \quad (20c)$$

201 and ultimately for the macroscopic potential

$$202 \quad M = S'_{i,J_l < 0} Q_s^{-1} + M_b \quad (21).$$

$$203 \quad F = (M - M_b) = S'_{i,J_l < 0} Q_s^{-1} \quad (22)$$

204 and

$$205 \quad \lambda = S'_{i,J_l < 0} F^{-2} \quad (23)$$

206 Note, M and F reflect values for each of the two half-spaces separated by a no-flow boundary condition

207 e.g. $F = (S'_{i,J_l < 0}/2)(Q_s/2)^{-1}$, which is true for a homogeneous profile only and is equivalent to the case

208 $J_l < 0$ above. The entropy production is calculated also with

$$209 \quad S'_{i,J_l < 0} = \int \sigma = \int (\sum qf) = \int \left(\sum \frac{1}{\alpha} \rho \frac{K}{v} k_r(\psi) (\mu_{high} - \mu_{low})^2 \right).$$

210 For a heterogeneous profile and/or $M_l > M_r$ (figure 4) i.e. when there is no symmetry

$$211 \quad M Q_s - J_l M_l - J_r M_r = S'_{i,J_l < 0} \quad (24).$$

212 Thus, the effective potential M of the cross section may be obtained from

213 $M = Q_s^{-1}(S'_{i,J_l < 0} + J_l M_l + J_r M_r)$ (25)

214 Additionally, expressions can be obtain for the conductance coefficients in the exchange with the left
 215 and right boundary conditions that are

216 $\lambda_l = (M Q_s - S'_{i,J_l < 0} - J_r M_r)(F_l M_l)^{-1}$ (26a)

217 $\lambda_r = (M Q_s - S'_{i,J_l < 0} - J_l M_l)(F_r M_r)^{-1}$ (26b).

218 where the macroscale forces $F_r = M - M_r$ and $F_l = M - M_l$ result from the differences between M and
 219 M_l, M_r with M following from equation 25. Again, entropy production is calculated with

220 $S'_{i,J_l < 0} = \int \sigma = \int (\sum qf) = \int \left(\sum \frac{1}{\alpha} \rho \frac{K}{v} k_r(\psi) (\mu_{high} - \mu_{low})^2 \right).$

221 For $J_l > 0$ (figure 5), the entropy balance is

222 $M Q_s + J_l M_l - J_r M_r = S'_{i,J_l > 0}$ (27)

223 and the macroscopic potential is

224 $M = Q_s^{-1}(S'_{i,J_l > 0} - J_l M_l + J_r M_r)$ (28)

225 With $Q_s = J_r - J_l$ follows

226 $J_l(M_l - M) + J_r(M - M_r) = S'_{i,J_l > 0}$ (29)

227 Thus, two conductances can be obtained, which are

228 $\lambda_l = (S'_{i,J_l > 0} - J_r(M - M_r)) F_l^{-2}$ (30)

229 $\lambda_r = (S'_{i,J_l > 0} - J_l(M_l - M)) F_r^{-2}$ (31)

230 with the macroscopic forces $F_l = (M_l - M)$ and $F_r = (M - M_r)$. In this example, two additional
 231 conductances can be obtained for the subdomains separated by the dividing streamline due to recharge
 232 shown in figure 5 that are

$$233 \quad \lambda_{Q_s} = \left(S'_{i,J_l>0} - J_l(M_l - M_r) \right) F_{Q_s}^{-2} \quad (32)$$

$$234 \quad \lambda_{l,r} = \left(S'_{i,J_l>0} - Q_s(M - M_r) \right) F_{l,r}^{-2} \quad (33)$$

235 with $J_r = J_l + Q_s$, and the macroscale forces $F_{Q_s} = (M - M_r)$ and $F_{l,r} = (M_l - M_r)$. In the domain, the
 236 entropy production is calculated also with

$$237 \quad S'_{i,J_l>0} = \int \sigma = \int (\sum qf) = \int \left(\sum \frac{1}{\alpha} \rho \frac{K}{v} k_r(\psi) (\mu_{high} - \mu_{low})^2 \right).$$

238

239 *Example 3:*

240 In this example, a no-flow boundary condition on the left is considered resembling a hillslope with a no-
 241 flow boundary along a hypothetical ridge on the left side, and a Dirichlet boundary condition along a
 242 hypothetical stream on the right side. Now, a source/sink $Q_s(x,t)$ varies periodically in space and time
 243 (periodically varying recharge/discharge). In this case, equation 2 needs to be solved for the different
 244 variables and integrated over one complete cycle at dynamic equilibrium.

245 Note, again $\int_0^L \nabla \cdot J dx = Q_s$, because there is a macroscopic, transient source/sink in the domain,
 246 therefore, after integration along the cross-section, the entropy balance reads

$$247 \quad S' + MQ_s - J_r M_r = S'_i \quad (34)$$

248 where S' is the entropy change rate. After time integration over one full cycle at dynamic equilibrium,
 249 $\overline{Q_s} = 0$ and $\overline{S'} = 0$, the effective macroscopic potential of the cross-section due to the periodic varying
 250 source/sink is

$$251 \quad \overline{M} = \overline{(S'_i + J_r M_r - S')} Q_s^{-1} \quad (35a)$$

252 or

$$253 \quad \overline{M} = \text{cov}(S'_i, Q_s^{-1}) + \overline{S'_i} \overline{Q_s^{-1}} + M_r (\text{cov}(J_r, Q_s^{-1}) + \overline{J_r} \overline{Q_s^{-1}}) + \text{cov}(S', Q_s^{-1}) \quad (35b)$$

254 based on the definition of the covariance.

255 Recognizing that $J_r = \int_0^L (Q_s - \Theta') dx$, where Θ' is the macroscopic mass change rate of the cross-
 256 section, one obtains for the effective force

$$257 \quad \overline{F} = \overline{(S'_i - \Theta' M_r - S')} Q_s^{-1} \quad (36a)$$

258 or

$$259 \quad \overline{F} = \text{cov}(\sigma, Q_s^{-1}) + \overline{\sigma} \overline{Q_s^{-1}} - M_r \text{cov}(\Theta', Q_s^{-1}) + \text{cov}(s', Q_s^{-1}) \quad (36b)$$

260 with $\overline{\Theta'} = 0$ due to dynamic equilibrium; and for the effective conductance

$$261 \quad \overline{\lambda} = \overline{(S'_i - \Theta' M - S')} F^2 \quad (37a)$$

262 or

$$263 \quad \overline{\lambda} = \text{cov}(S'_i, F^2) + \overline{S'_i} \overline{F^2} - \text{cov}(\Theta' M, F^2) + \overline{\Theta' M} \overline{F^2} + \text{cov}(S', F^2) \quad (37b)$$

264 with $J_r = \lambda F = \lambda(M - M_r)$.

265 Apparently, on the right hand side of equations 35, 36, and 37 all terms may be calculated from the
 266 numerical simulations except the entropy change rate $S' = \int s'$ and therefore also $\text{cov}(S', Q_s^{-1})$, because

267 both, S' and M are not known in equation 34 (note, S'_i is calculated explicitly). However, S' is needed in
 268 the estimation of \bar{F} and $\bar{\lambda}$ and may actually be calculated from the microscale variables, which is
 269 demonstrated with a discrete example depicted in the schematic in figure 6.

270 In this schematic, there are three microscale elements with sources/sinks in each individual element (q_l ,
 271 q_c , q_r) and a constant potential boundary condition on the right (μ_b). For each individual element the
 272 entropy balance is

$$273 \quad s'_l + q_l \mu_l - q_{l,c} \mu_{l,c} = \sum q_l f_l = q_{l,c} (\mu_l - \mu_{l,c}) \quad (38a)$$

$$274 \quad s'_c + q_c \mu_c + q_{l,c} \mu_{l,c} - q_{c,r} \mu_{c,r} = \sum q_c f_c = q_{l,c} (\mu_{l,c} - \mu_c) + q_{c,r} (\mu_c - \mu_{c,r}) \quad (38b)$$

$$275 \quad s'_r + q_r \mu_r + q_{c,r} \mu_{c,r} - q_b \mu_b = \sum q_r f_r = q_{c,r} (\mu_{c,r} - \mu_r) + q_b (\mu_r - \mu_b) \quad (38c)$$

276 where the fluxes and potentials with the subscript l,c and c,r are valid at the element interfaces. The
 277 terms on the right hand side i.e. the entropy production for each element encompass the fluctuations in
 278 the flux-force relationships between the element's interior and the element boundaries. Summation of
 279 the individual balance equations leads to the total balance

$$280 \quad s' + q_l \mu_l + q_c \mu_c + q_r \mu_r - q_b \mu_b = \sigma = q_{l,c} (\mu_l - \mu_c) + q_{c,r} (\mu_c - \mu_r) + q_b (\mu_r - \mu_b) \quad (39).$$

281 Note, on the left hand side, all the interface terms disappear and only the source and boundary terms
 282 remain, equivalent to the macroscale balance in equation 34. Equation 38 is the entropy balance
 283 equation for the system depicted in figure 6.

284 Any changes in the entropy of the system with time are due to transient effects that cancel out at
 285 dynamic equilibrium $\bar{s}' = 0$. In order to demonstrate this, substitution of $q_{l,c} = (q_l - \theta'_l)$, $q_{c,r} =$
 286 $(q_l - \theta'_l) + (q_c - \theta'_c)$, and $q_b = (q_l - \theta'_l) + (q_c - \theta'_c) + (q_r - \theta'_r)$ for the interface fluxes on the right
 287 hand side in equation 38 leads to

$$s' + q_l \mu_l + q_c \mu_c + q_r \mu_r - q_b \mu_b =$$

$$(q_l - \theta'_l) \mu_l + (q_c - \theta'_c) \mu_c + (q_r - \theta'_r) \mu_r - q_b \mu_b \quad (40)$$

289 which demonstrates continuity in case of steady state $\theta'_l = \theta'_c = \theta'_r = 0$, and shows that any e.g.
 290 positive mass storage change θ' over the microscopic volume leads to negative change in entropy and
 291 vice versa. Note, the entropy production is still always positive as required by definition. Thus, S' and M
 292 can be evaluated by applying equation 39 to microscale simulations.

293 A special case may be considered, in which the system depicted in figure 6 is also closed on the right side
 294 resulting in a sole exchange with the surroundings via the periodic source/sink (e.g.
 295 infiltration/evapotranspiration) $Q_s(t)$. This would be equivalent to a profile with a discharge area in the
 296 center and the assumption of symmetry shown in the schematic in figure 7. The requirement again is
 297 that $\overline{Q_s} = 0$ over one full cycle at dynamic equilibrium. Then e.g. equation 35 simplifies to

$$\overline{M} = \overline{(S'_i - S') Q_s^{-1}} \quad (41a)$$

299 or

$$\overline{M} = \text{cov}(\Delta S', Q_s^{-1}) + \overline{S'_i Q_s^{-1}} \quad (41a)$$

301 with $\Delta S' = S'_i - S'$.

302

303 Discussion

304 The major advantage of the proposed inference theory is the estimation of macroscopic variables that
 305 are thermodynamically consistent with the microscale fluctuations. This is discussed in the context of the
 306 simple example 1 interpreting the entropy current $J_s = JM$ as an advective potential flux. Because J is
 307 constant and $M_l > M_r$, the entropy current leaving the domain on the right side is smaller than the

308 entropy current entering the domain on the left side. This is due to dissipation in the interior of the
 309 domain resulting into the production of entropy S'_i . In hydrology, the dissipation is simulated using
 310 Darcy's law and Richards equation at the support (here microscopic) scale, where all dissipative
 311 processes are lumped in the hydraulic conductivity representing the flow resistance. Thus, at the
 312 macroscale the derived conductance λ is thermodynamically consistent if one accepts e.g., Darcy's law as
 313 a valid parameterization of the internal dissipative processes. Note, in this study, J_s is equivalent to the
 314 internal energy current in the energy balance equation, because temperature is constant.

315 Equations 12 and 13 have not been applied before in the context of hydrology. While the equations
 316 illustrate the basic idea for the simplest case of a Darcy experiment, one may argue that the insight
 317 gained from this example is rather limited, because λ could have been obtained from the known flux-
 318 force relationship and the conductance equation (one unknown λ with one equation 7). Examples 2 and
 319 3, on the other hand, clearly illustrate the advantage, because the macroscale potential M (and
 320 therefore F), which are needed to obtain λ are not known in these examples. Thus, one is left with two
 321 unknowns λ and F , and only one equation (the conductance equation 7). In the proposed theory, the
 322 entropy balance provides the second equation to solve for the two unknowns at the cost of explicitly
 323 calculating the internal entropy production $S'_i = \int \sigma = \int (\sum qf) = \int \left(\sum \frac{1}{\alpha} \rho \frac{K}{v} k_r(\psi) (\mu_{high} - \mu_{low})^2 \right)$,
 324 and at the benefit of thermodynamic consistency. This is the central message of the proposed method of
 325 inference, which exploits the internal entropy production S'_i as a spatial and also temporal integrator.

326 It is important to emphasize that one can also obtain, in an ad hoc fashion, the forces and conductance
 327 coefficients for any sub-domain V_i of the global domain with volume V . For example, in order to obtain
 328 the macroscale potential in the center of the profile of example 1, one arrives at

$$329 \quad M_c = M_l - J^{-1} \int_{V_i} \sigma dV_i \quad (42).$$

330 Thus, from $\int_{V_i} \sigma dV_i$ estimates, one is able to obtain macroscale variables over a hierarchy of scales for
331 different hydrologic configurations similar to the simple examples provided above.

332 Under purely saturated groundwater flow conditions, the estimates of macroscale variables can be used
333 directly for predictions, because λ is constant for the same flow geometries, which is trivial, but
334 important to realize. In case of variably saturated flow and transient conditions (when the flow geometry
335 changes), λ is of course not constant and S'_i will depend in an unknown, non-linearly fashion on the flux J
336 and its variability (example 3), which apparently limits the usefulness of the proposed approach.

337 However, universal relationships of $S'_i(J)$ and $\text{cov}(S'_i, J^{-1})$ can perhaps be obtained from a series of
338 numerical experiments under characteristic hydrologic configurations.

339 This also brings up the question, whether one is able to establish a connection of the proposed theory
340 with observations of real-world systems. Obviously, S'_i can not be measured directly in the field utilizing
341 independent experiments, which could, in turn, be used to derive macroscopic thermodynamic forces
342 from flux observations that are more readily available. Thus, utilizing the entropy balance for estimating
343 macroscopic field variables and ensuing predictions appears limited at this point. Yet, this study suggests
344 exploring relationships of measurable field variables and S'_i utilizing numerical experiments, in future. In
345 turn, under certain conditions, estimates of S'_i from measurable quantities may be possible. With the
346 help of the extended example 1, this is discussed below.

347 Assuming a time varying force i.e. Dirichlet boundary conditions, temporal integration of equation 11
348 over one full cycle at dynamic equilibrium yields

$$349 \quad \bar{S}'_i = \bar{JF} \quad (43)$$

350 Inserting the conductance equation into equation 43 under saturated, linear groundwater flow
351 conditions with the assumption of only small changes in the flow geometry (λ is constant) leads to

352 $\bar{S}'_i = \lambda^{-1} \bar{J}^2 = \lambda^{-1} [\text{var}(J) + \bar{J}^2]$ (44).

353 Thus, entropy production is related inversely to λ , linearly to $\text{var}(J)$, and power two to \bar{J} If an estimate
354 of λ is available, \bar{S}'_i can be calculated from observations of J . In the more realistic case of variably
355 saturated groundwater flow and/or varying flow geometry, equation 44 changes to

356 $\bar{S}'_i = \overline{\lambda^{-1} J^2} = \text{cov}(\lambda^{-1}, J^2) + \overline{\lambda^{-1}} \bar{J}^2$ (45).

357 illustrating the same dependence of \bar{S}'_i on $\bar{\lambda}$ and \bar{J} as before. The unknown covariance $\text{cov}(\lambda^{-1}, J^2)$ may
358 potentially be estimated from numerical experiments.

359

360 **Summary and conclusions**

361 In this study, the method of inference based on the entropy balance equation was introduced. The
362 theoretical basis is the explicit calculation of the internal microscale entropy production, which is used in
363 the balance equation to solve for macroscale potentials, and thermodynamic forces and fluxes. The
364 proposed method was illustrated with simple hydrologic cross-sections of steady-state, variably saturated
365 groundwater flow and a periodic source/sink (infiltration/evapotranspiration) at dynamic equilibrium.

366 The entropy balance equation is remarkable, because the equation unifies the macro- and microscale in
367 one equation allowing the simultaneous application of two different movement equations that are the
368 conductance equation at the macroscale and Darcy's law/Richards equation at the microscale, in this
369 study. The derivations lead to expressions for macroscale variables that are a function of the entropy
370 production (i.e. the internal fluctuations of the microscale flux-force relationships) and provide a
371 thermodynamically consistent link between the two different scales. Therefore, the derivation provides a
372 different theoretical perspective of variably saturated groundwater flow and new approaches for
373 obtaining effective macroscale variables. The discussion suggests that these may be derived consistently

374 for a hierarchy of scales. With the advent of high-performance computing in hydrology, there is strong
375 potential for additional insight from hyper-resolution numerical experiments to explicitly calculate the
376 internal entropy production. For example, existing and new averaging and upscaling laws may be tested
377 and derived using series of numerical experiments with e.g. varying subsurface heterogeneity
378 configurations, and boundary conditions. These experiments may also be useful in deriving new
379 movement equations at the macroscale replacing empirical, calibrated parameterizations and
380 regionalization approaches.

381 The study is a contribution to the field of *theoretical hydrology*, providing a thermodynamic perspective
382 of inference in hydrology. While inference of macroscale variables necessitates explicit calculation of the
383 entropy production and thus considerable computational resources, these resources are well-invested:
384 Obtaining previously unknown macroscale parameters is at the center of the ubiquitous challenge of
385 upscaling and applying the proposed framework may help in finding general upscaling relationships over
386 a hierarchy of scales. The connection to real-world observations needs to be established in future, also
387 with the help of numerical simulations. In the provided theoretical setting, the usefulness of the method
388 for predictions is evident from the simple examples provide here, however, for real-world predictions
389 this remains to be demonstrated.

390

391 **Acknowledgements**

392 I would like to thank the Associate Editor Murugesu Sivapalan, and the reviewers Stan Schymanski,
393 Martijn Westhoff, Erwin Zehe and one anonymous reviewer for their constructive comments and
394 suggestions during the review process. I also would like to thank Elbert Branscomb for initial and Axel
395 Kleidon for more extensive discussions.

396

397 **References**

- 398 Dewar, R. (2003) Information theory explanation of the fluctuation theorem, maximum entropy
399 production and self-organized criticality in non-equilibrium stationary states. *Journal of Physics a-*
400 *Mathematical and General* 36(3), 631-641.
- 401 Koutsoyiannis, D. (2014) Entropy: From Thermodynamics to Hydrology. *Entropy* 16(3), 1287-1314.
- 402 Zehe, E., Ehret, U., Blume, T., Kleidon, A., Scherer, U. and Westhoff, M. (2013) A thermodynamic
403 approach to link self-organization, preferential flow and rainfall-runoff behaviour. *Hydrology and Earth*
404 *System Sciences* 17(11), 4297-4322.
- 405 Ehret, U., Gupta, H.V., Sivapalan, M., Weijs, S.V., Schymanski, S.J., Blöschl, G., Gelfan, A.N., Harman, C.,
406 Kleidon, A., Bogaard, T.A., Wang, D., Wagener, T., Scherer, U., Zehe, E., Bierkens, M.F.P., Di Baldassarre,
407 G., Parajka, J., van Beek, L.P.H., van Griensven, A., Westhoff, M.C. and Winsemius, H.C. (2014) Advancing
408 catchment hydrology to deal with predictions under change. *Hydrology and Earth System Sciences* 18(2),
409 649-671.
- 410 Dewar, R.C. (2010) Maximum entropy production and plant optimization theories. *Philosophical*
411 *Transactions of the Royal Society B-Biological Sciences* 365(1545), 1429-1435.
- 412 Miedziejko, E.M. and Kedziora, A. (2014) Impact of plant canopy structure on the transport of ecosystem
413 entropy. *Ecological Modelling* 289, 15-25.
- 414 del Jesus, M., Foti, R., Rinaldo, A. and Rodriguez-Iturbe, I. (2012) Maximum entropy production, carbon
415 assimilation, and the spatial organization of vegetation in river basins. *Proceedings of the National*
416 *Academy of Sciences of the United States of America* 109(51), 20837-20841.
- 417 Paillard, D. and Herbert, C. (2013) Maximum Entropy Production and Time Varying Problems: The
418 Seasonal Cycle in a Conceptual Climate Model. *Entropy* 15(7), 2846-2860.
- 419 Abe, S. and Okuyama, S. (2011) Similarity between quantum mechanics and thermodynamics: Entropy,
420 temperature, and Carnot cycle. *Physical Review E* 83(2).

421 Kleidon, A., Zehe, E., Ehret, U. and Scherer, U. (2013) Thermodynamics, maximum power, and the
422 dynamics of preferential river flow structures at the continental scale. *Hydrology and Earth System
423 Sciences* 17(1), 225-251.

424 Westhoff, M.C., Zehe, E. and Schymanski, S.J. (2014) Importance of temporal variability for hydrological
425 predictions based on the maximum entropy production principle. *Geophysical Research Letters* 41(1), 67-
426 73.

427 Kleidon, A. and Schymanski, S. (2008) Thermodynamics and optimality of the water budget on land: A
428 review. *Geophysical Research Letters* 35(20).

429 Westhoff, M.C. and Zehe, E. (2013) Maximum entropy production: can it be used to constrain conceptual
430 hydrological models? *Hydrology and Earth System Sciences* 17(8), 3141-3157.

431 Porada, P., Kleidon, A. and Schymanski, S.J. (2011) Entropy production of soil hydrological processes and
432 its maximisation. *Earth System Dynamics* 2(2), 179-190.

433 Schymanski, S.J., Kleidon, A., Stieglitz, M. and Narula, J. (2010) Maximum entropy production allows a
434 simple representation of heterogeneity in semiarid ecosystems. *Philosophical Transactions of the Royal
435 Society B-Biological Sciences* 365(1545), 1449-1455.

436 Klausmeier, C.A. (1999) Regular and irregular patterns in semiarid vegetation. *Science* 284(5421), 1826-
437 1828.

438 Dewar, R.C. (2009) Maximum Entropy Production as an Inference Algorithm that Translates Physical
439 Assumptions into Macroscopic Predictions: Don't Shoot the Messenger. *Entropy* 11(4), 931-944.

440 Kresse, G. and Hafner, J. (1994) Ab-Initio Molecular-Dynamics Simulation of the Liquid-Metal
441 Amorphous-Semiconductor Transition in Germanium. *Physical Review B* 49(20), 14251-14269.

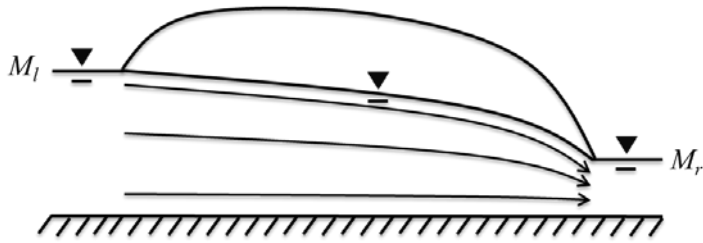
442 Kondepudi, D. and Prigogine, I. (2015) *Modern Thermodynamics: From Heat Engines to Dissipative
443 Structures*, 2nd Edition. *Modern Thermodynamics: From Heat Engines to Dissipative Structures*, 2nd
444 Edition, 1-523.

445

446

447 **Figures**

448



449

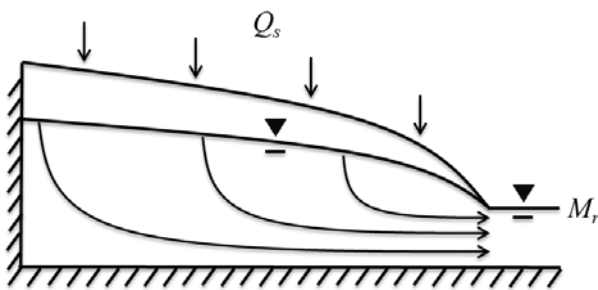
450 Figure 1. Schematic of a simple profile with Dirichlet boundary conditions on the right and left (M_r, M_r)

451 and steady state variably saturated flow. In the theory, the vertical and horizontal extents of the cross-

452 section are assumed to be constant.

453

454



455

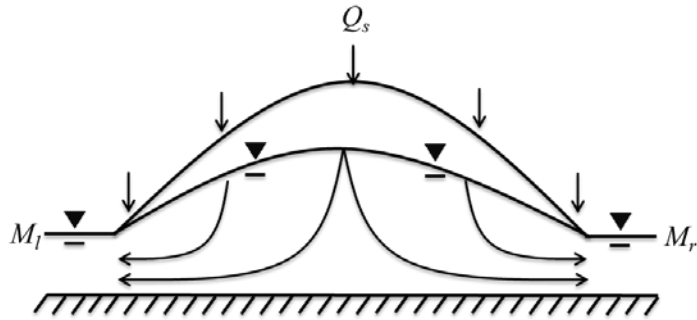
456 Figure 2. Schematic of a simple profile with a Dirichlet boundary condition on the right (M_r), a no-flow

457 boundary condition on the left, a constant source (Q_s), and steady state variably saturated groundwater

458 flow. In the theory, the vertical and horizontal extents of the cross-section are assumed to be constant.

459

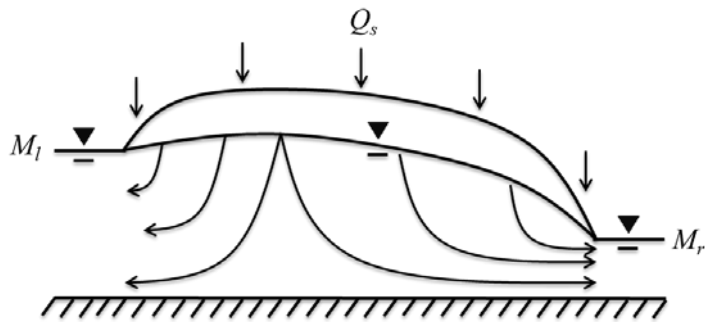
460



461

462 Figure 3. Schematic of a simple profile with Dirichlet boundary conditions on the right and left (M_l, M_r) a
463 constant source (Q_s), and steady state variably saturated groundwater flow. In this symmetric case,
464 there exist a water divide in the center of the domain. In the theory, the vertical and horizontal extents
465 of the cross-section are assumed to be constant.

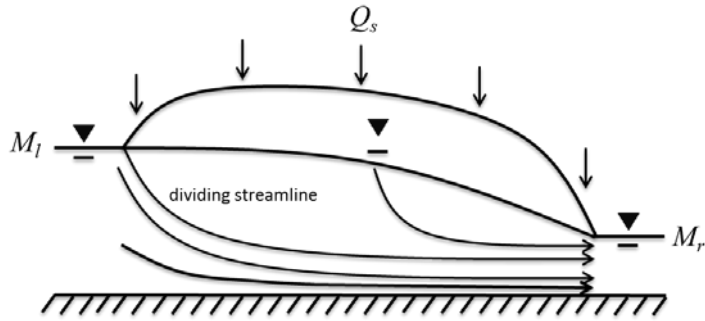
466



467

468 Figure 4. Schematic of a simple profile with Dirichlet boundary conditions on the right and left (M_l, M_r) a
469 constant source (Q_s), and steady state variably saturated flow. In this case there exist a water divide in
470 the domain. In the theory, the vertical and horizontal extent of the cross-section is assumed to be
471 constant.

472

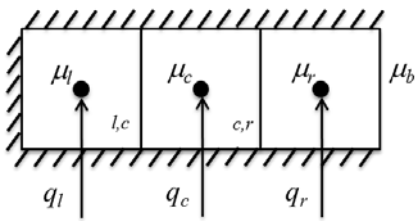


473
 474 Figure 5. Schematic of a simple profile with Dirichlet boundary conditions on the right and left (M_l, M_r), a
 475 constant source (Q_s), and steady state variably saturated groundwater flow. Note the dividing streamline
 476 in this example. In the theory, the vertical and horizontal extents of the cross-section are assumed to be
 477 constant.

478

479

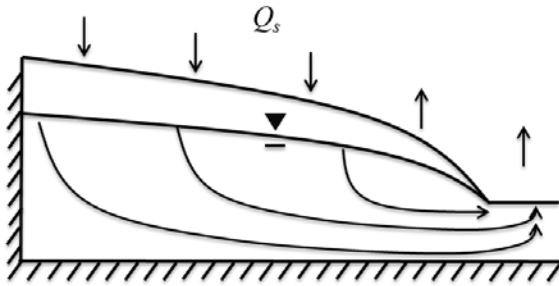
480



481
 482 Figure 6. Schematic of the discrete example consisting of three microscale elements with a Dirichlet
 483 boundary condition on the right side (μ_b) and a source/sink in each element (q_l, q_c, q_r).

484

485



486

487 Figure 7. Schematic of a simple profile with a no-flow boundary condition on the left and right (based on
488 symmetry) and transient, spatially varying sources/sinks $Q_s(x, t)$ resulting in a recharge and discharge
489 area. In the theory, the vertical and horizontal extent of the cross-section is assumed to be constant.

490